

# Measuring the Mean Lifetime of Cosmic Muons

Jason R. Heimann  
and  
John Wray

December 6, 2004

# Contents

<b>1</b>	<b>Introduction</b>	<b>1</b>
<b>2</b>	<b>Experimental Apparatus</b>	<b>1</b>
2.1	Absorber . . . . .	1
2.2	Counters . . . . .	2
2.3	Electronic modules . . . . .	2
2.3.1	Discriminator . . . . .	3
2.3.2	Logic . . . . .	3
2.3.3	Gate generator . . . . .	3
2.3.4	Time to amplitude converter . . . . .	4
2.4	Data acquisition system . . . . .	4
2.5	Other equipment . . . . .	4
<b>3</b>	<b>Procedure</b>	<b>4</b>
3.1	Calibration . . . . .	5
3.2	Counter characterization . . . . .	5
3.3	Logic setup . . . . .	6
3.4	Measurement . . . . .	6
<b>4</b>	<b>Results</b>	<b>6</b>
4.1	Calibration . . . . .	6
4.2	Counter characterization . . . . .	6
4.3	Measurement . . . . .	7
<b>5</b>	<b>Analysis and Interpretation</b>	<b>7</b>
5.1	Theory . . . . .	7
5.2	Experiment . . . . .	8
<b>6</b>	<b>Conclusion</b>	<b>9</b>
<b>7</b>	<b>Tables and Figures</b>	<b>9</b>

# List of Tables

1	Results of TAC / MCA calibration . . . . .	9
2	Details of linear fit . . . . .	11
3	Results of 100 sec. of measurement with PMT A at three thresholds . . . . .	13
4	Results of 100 sec. of measurement with PMT B at three thresholds . . . . .	14
5	Results of 100 sec. of measurement with PMT C at three thresholds . . . . .	15
6	Results of 100 sec. of measurement with PMT D at three thresholds . . . . .	16
7	Efficiency measurements for counter A . . . . .	19
8	Efficiency measurements for counter B . . . . .	19
9	Efficiency measurements for counter C . . . . .	20
10	Efficiency measurements for counter D . . . . .	20

11	Operating parameters for counters . . . . .	20
12	Coincidence rates from counters in experimental configuration . . . . .	20
13	Re-binned results of experiment . . . . .	23
14	Details of curve fit . . . . .	23

## List of Figures

1	The distribution of electron kinetic energies in muon decay at rest. Data from the experiment of Bardon <i>et al.</i> (1965). Experimental points are compared to a modified theoretical curve. . . . .	10
2	Detail of experimental setup, side view. Counters C and D are above absorber, counters A and B are below. Absorber is described in Section 2.1. . .	10
3	Schematic of experimental setup. Connections within the NIM crate are described in Section 3.3. . . . .	11
4	Schematic of electrical configuration. Inputs from PMTs are indicated at left, outputs to TAC appear at right. . . . .	11
5	Results of TAC / MCA calibration, plus linear fit (note: TOF is Time Of Flight) . . . . .	12
6	Schematic of counter efficiency calibration . . . . .	12
7	Plot of 100 sec. measurements for PMT A . . . . .	17
8	Plot of 100 sec. measurements for PMT B . . . . .	17
9	Plot of 100 sec. measurements for PMT C . . . . .	18
10	Plot of 100 sec. measurements for PMT D . . . . .	18
11	Plot of efficiencies of PMT A . . . . .	21
12	Plot of efficiencies of PMT B . . . . .	21
13	Plot of efficiencies of PMT C . . . . .	22
14	Plot of efficiencies of PMT D . . . . .	22
15	Results of experiment, with curve fit . . . . .	24

### *Abstract*

An experiment is designed to measure the lifetime of the cosmic muon. The photo-multiplier tubes and electronics used in the experiment are characterized and parameters are optimized for maximum efficiency. The observed lifetimes are fit with a curve to determine a mean lifetime of  $2.10 \text{ uS} \pm 0.05 \text{ uS}$ .

# 1 Introduction

Philosophers in Ancient Greece took their part in the study of particle metaphysics by postulating the existence of matter in discrete, irreducible quanta they called “atoms.” Many centuries later, physicists discovered the constituents of atoms, known as subatomic particles. The overwhelming body of experimental evidence available today tells us that all matter is composed of three fundamental particles: the proton, neutron and electron.

What makes these three particles special? The proton, neutron and electron are the most stable particles observed by man. Physicists have discovered dozens upon dozens of “new” particles since the advent of the particle accelerator. These new particles require great amounts of energy to produce, and even then they only last for a tiny fraction of a second (on the order of  $10^{-10}$  seconds) before decaying. In comparison, the electron has a lifetime of *at least*  $10^{26}$  years! [1]

In this experiment we make use of astrophysical particle accelerators to study a short-lived relative of the electron: the muon. When high-energy particles from outer space collide with the Earth’s upper atmosphere, various exotic particles are produced that decay quickly. Muons are a common by-product of these decays, and some muons are given enough kinetic energy to travel to the Earth’s surface before they decay.

Upon the decay of a muon, an electron is emitted in its place, often with sufficient kinetic energy to send it through several meters of air (or a decimeter of most dense materials) before stopping. Our experiment aims to “capture” cosmic muons and time the emission of the resultant electron. Many muon decays must be observed to make a statistically significant measurement of mean lifetime.

## 2 Experimental Apparatus

An individual particle can not provide enough stimulus to elicit a reaction from any human sense, so indirect methods must be used to study fundamental particles. Some indirect methods, including those used since the early 1900’s [2], employ a target, barrier or absorber with which the particle(s) will interact. Those interactions are then studied to uncover fundamental truths about the particle(s) under study.

### 2.1 Absorber

To capture a cosmic muon we need to absorb its kinetic energy such that it slows to a stop inside our experiment. We choose our absorber material for its electron density (or small nuclei / low Z), as muons passing through this material will interact primarily with atomic electrons[1]. In these interactions the atoms become excited or ionized, and the muon loses some energy as a result. We design the absorber to be large enough to stop cosmic muons, but not so large that we also stop the decay electrons from escaping!

The Bethe-Bloch equation gives the mean rate of energy loss (or stopping power) in matter as a function of many variables including the atomic number of the matter and the incident particle’s charge and speed. To summarize this equation and the units which we

will see in our data:

$$-\frac{dE}{dx} \propto Kz^2 \frac{Z}{A} \frac{1}{\beta^2} \quad (1)$$

$$\left[ -\frac{dE}{dx} \right] = \left[ \frac{\text{MeV} \cdot \text{cm}^2}{\text{g}} \right] \quad (2)$$

We use predetermined results from this equation for our experiment, but what we take from it is the relationship between material density, particle speed and stopping power. From the spectrum of decay electron momenta (see Figure 1 [4]) we determined the absorber should be about 60 MeV “in diameter.” That is, an electron emitted in the center of the absorber should not lose more than 30 MeV before escaping.

We used a rough estimate of the stopping power of  $2.2\text{MeVcm}^2\text{gm}^{-1}$  and assumed a specific gravity of unity [3] to determine our radius:  $60\text{MeV}/(1.00\text{gcm}^3 \cdot 2.2\text{MeVcm}^2\text{g}^{-1}) = 27\text{cm}$ . Finally, we constructed a 29.5 cm H x 28 cm W x 62 cm L absorber by stacking books upon each other.

## 2.2 Counters

Immediately surrounding our absorber are four “counters,” each comprised of a plastic scintillator optically joined to a photo-multiplier tube and wrapped in thin, opaque material. The counter’s job is to signal when a charged particle passes through the scintillator. The actual signal coming from the counter is a small “tail pulse,” typically -100 mV in amplitude (all signals are negative) and a few 10s of nanoseconds in duration. To distinguish the counters used in our experiment, we have labeled them with the Roman letters A, B, C and D.

As in our absorber, cosmic muons (and electrons) will pass through each scintillator, exciting some of the atoms in the plastic. As these atoms relax, they will emit optical photons; the scintillators in our experiment will yield a few hundred photons in response to a typical particle event. Through total internal reflection, the photons eventually make it to one “end” of the scintillator, where they can be detected. The scintillators cover a horizontal area of about 60 x 25 cm and are 1 cm thick. Two scintillators were used on either side of the absorber; see Figure 2 for a schematic of our setup.

A photo-multiplier tube (PMT) is employed to detect the photons emitted within the scintillator. The PMT relies on the photoelectric effect and a strong electric field to produce accelerated electrons from the few incoming photons. Multiple dynodes held at increasing potentials create a cascade effect, amplifying the number of particles incident on the PMT. The electrons are collected at an anode at the rear of the PMT, and are presented through a BNC connector on the PMT base. A high-voltage power supply is used to bias each PMT; the tubes require up to 2000V of bias power but consume very little current (about 1 mA).

## 2.3 Electronic modules

The signals coming from the PMTs vary in height and width, depending on the amount of energy deposited in the scintillator. Note the scintillator does not care about the charge or the mass of the particle, it only responds to energy deposition (formally,  $dE/dX$ , as in

Equation 1). In addition to particle signals, the output from the PMT includes several types of electrical noise.

Specialized electronic modules must be used to extract valid signals from noise and background events. The actual electronic modules used are known as NIM modules (Nuclear Instrumentation Methods), and a “NIM crate” is provided to power these modules. The modules are compact and reconfigurable within the crate; they are joined by various lengths of cabling with quick-release “LEMO” style connectors. Signal propagation times within these cables have been measured and their approximate values (typ. 2, 4, 8) in nanoseconds are marked on the insulation of each cable.

### 2.3.1 Discriminator

We used a LeCroy Quad Discriminator (Model 821), containing four discriminator circuits. A discriminator inputs PMT signals and outputs a well-defined pulse for selected inputs. Each discriminator has an adjustable threshold which may be set from -30 mV to about -2 V. Input signals that swing below the threshold trigger an output pulse, -800 mV in amplitude and 50 nS in width (known as a NIM pulse). Discriminators are used to “ignore” noise signals while passing particle signals.

### 2.3.2 Logic

We stacked two counters on each other to acquire “coincidence” signals (see Figure 2). Random fluctuations of noise in a PMT can trigger a discriminator, producing a false event. To avoid measuring false events, we required signals from two adjacent counters that were coincident in time. For such a requirement we used the LeCroy 4-fold Logic Unit (model 365AL). This module outputs a NIM pulse when a selected number of coincident NIM pulses (also known as a “coincidence level”) appear at any of the four inputs. The output pulse can be suppressed by a “veto” signal, also a NIM logic input.

If the coincidence level is set to one, the logic unit acts as an OR gate, producing an output when any input is activated (and the “veto” signal is not present, assume this from now on). We connected two adjacent counters to a logic unit with a coincidence level of two to produce coincidence signals; this configuration was an effective AND gate. Both OR and AND gates appeared in our experimental setup, see Figure 4. It should be noted that each logic unit adds 10 nS of delay in the signal path.

### 2.3.3 Gate generator

We used two Joerger model GG gate generators in two different roles in this experiment. In theory, a gate generator acts much like a discriminator, outputting a NIM pulse with a preselected width immediately upon receiving an input pulse. With some additional outputs, the gate generator can also act like a delay line, outputting a pulse at some predefined interval after the input pulse.

The gate generator was used to define the window of time in which we look for muon decay events. Events from high-energy muons that pass through the experiment without decaying created two coincidence signals in a very short interval. A 100 nS delay was incorporated to ignore these events. A 10  $\mu$ S gate was connected after the delay to define

the ceiling for lifetime measurements. This setup is described in more detail below (see Section 3.3).

#### 2.3.4 Time to amplitude converter

A Time to Amplitude Converter (TAC) module was used to convert lifetime measurements into analog voltages. This conversion enables slower data acquisition (DAQ) systems to capture relatively quick timing signals. The conversion is accomplished through two NIM logic inputs: “start” and “stop”. The time between a start signal and a stop signal is measured, then a fixed-width positive square pulse is output with an amplitude proportional to the measured time.

The module contains some logic to avoid improper measurements: sequential start pulses caused previous starts to be invalidated, and stops that appeared after the window of measurement (10uS) were ignored. This module also contains scaling controls to allow a range of measurements. We set the “Range” control to 100 nS and the “Mult[iplier]” control to 100, for an effective measurement range of  $100\text{nS} \times 100 = 10\text{uS}$ . The output of the TAC was connected directly to our DAQ system with a 2 m BNC cable.

### 2.4 Data acquisition system

A computer with a Multi-Channel Analyzer (MCA) card was used to record the signals output by the TAC. The height of each input pulse was analyzed and stored as a count in one of 2048 bins; each bin represented a range of input pulses  $\sim 5$  mV wide. The bin range was set within the software; for our experiment the “ADC Gain” was set to 2048. The raw data (counts in each bin) from our experiment was saved in a text file that was later analyzed with statistical software including Gnuplot and ROOT.

### 2.5 Other equipment

Common lab equipment was used to aid the configuration of our experiment. We used a Tektronix TDS 380 Digital Oscilloscope to view signals from the PMT and calibrate our NIM pulse widths (from discriminators, gates, etc.). A Keithley bench-top DMM is used to measure discriminator thresholds. A HP 5134 universal counter is used to make estimates of noise and signal rates, while a Jorway Model 1880B BCD scaler was employed when exact counts were required.

## 3 Procedure

Before our apparatus can be used to extract meaningful and accurate results, we had to characterize and configure several pieces of equipment. We needed to ensure the PMTs were biased with the proper voltage and were outputting valid and measurable signals. The discriminator thresholds were carefully selected to provide a minimum noise margin and avoid ignoring valid signals. We also had to fully understand the signals entering and exiting the TAC and how they were represented by the MCA software.

### 3.1 Calibration

To determine the physical meaning behind the output from the MCA software, we simulated decay events and recorded a small amount of data. A tail pulse generator (BNC model BH-1) with an adjustable delay was connected to the TAC inputs, and the MCA software collected the resulting signals. We used our oscilloscope to verify the time between the start and stop signals we generated, then we recorded the MCA bin in which these signals appeared.

It should be noted that this procedure was a simultaneous calibration of the TAC and the MCA hardware. Since these two individual pieces of hardware exhibit very linear responses to their inputs, we feel no “intermediate” calibration was required. As such, the MCA output can be interpreted as time signals, with each count representing one decay measurement.

### 3.2 Counter characterization

Our next step was to bias each PMT with the optimum voltage to achieve a good signal to noise ratio. Using several discriminators, a gate generator and several scalers, we counted cosmic rays for 100 seconds at three arbitrarily chosen thresholds (-30, -60 and -90 mV). This exercise was repeated for a range of bias voltages, using each counter (one at a time). The goal of this exercise is to find a range of bias voltages across which the count rate does not change appreciably. This would appear as a “plateau” in a graph of counts vs. bias voltage, often referred to as a “plateau curve.” The plateau voltage is the point at which we have achieved an optimum signal to noise ratio; this voltage was used to bias the PMT for the remainder of the experiment.

We then determined the correct discriminator threshold by measuring the counters’ efficiencies at various thresholds. This determination was made by counting coincidence signals (generated by various cosmic rays) in a “3-2” setup: three counters arranged such that the top and bottom counters overlap each other in an area equal to the width of the counter placed in the middle. See Figure 6 for a schematic of this setup. The counters are connected to discriminators set to fairly low thresholds for this exercise. In this configuration, we can detect when the middle counter (a.k.a. the Counter Under Test, CUT) *should* produce a signal. The assumption is: if we receive coincident signals from the top and bottom counters, there most likely was a particle passing through the overlapping area, and therefore we should see a coincident signal from the CUT.

Using logic units, we produced outputs for double (top and bottom) and triple signal coincidences, and then we counted these signals until we achieved at least 1000 double coincidences. The counts are compared as such: triple coincidences / double coincidences = CUT efficiency (in %). This procedure began with the CUT threshold at its lowest setting ( $\sim -30$  mV) and was repeated with increasing thresholds until we saw 20% efficiency or less. The “correct” threshold is chosen just above the “knee” in a graph of efficiency vs. threshold (see Figure 11 for an example). We chose this value to ensure maximum particle detection efficiency with the least amount of false triggers from noise.

After the counters and discriminators are set up, we had to do a quick check of counter signal rates (or “trigger rates”) to ensure our equipment was behaving as expected. To ensure a counter is not too noisy to provide reliable results, we verify its trigger rate is under 100 Hz. We then set the counters up for the experiment, as in Figure 2, and check the double coincidence rates in the top and bottom pairs of counters. The final configuration

used in our experiment is indicated in Figure 3.

### 3.3 Logic setup

In most particle physics experiments, logic is used as a first-order filter to select events of interest and reject background events. Figure 4 contains a schematic of the logic used in our experiment. Each counter's signal was run through a discriminator before arriving at a logic unit. We used double-coincidence signals as triggers, so an "AND" logic configuration is used for the top and bottom pairs of counters. The top pair produced the TAC start signal for our experiment, while either the top or bottom pair could produce the TAC stop signal. This required the use of an "OR" logic unit.

We used the veto feature of the OR logic unit to prevent a TAC stop signal from appearing too early or too late. The 100 nS delay held the veto signal high (preventing output) to ignore non-decay events, while the 10 uS gate held the veto signal low (allowing output) to accept signals within our window of measurement. To ensure accurate timing, we used various lengths of cabling in our setup to ensure start and stop signals traveled through the same "electrical length," that is, signals coming from any counter reach the TAC stop input in the same amount of time required to reach the TAC start input.

### 3.4 Measurement

Once the equipment was characterized and configured, the experiment practically ran itself. No further human intervention was required until it was time to turn the equipment off! The data acquisition system ran continuously throughout the experiment, recording events as they occurred. We "eyeballed" the data once a day throughout the experiment to make sure we collected no unintentional results (i.e. spurious peaks in the histogram).

We decided 10,000 events was an acceptable cut-off point for our experiment. This determination was a compromise between the time required to run the experiment and the error in our results:  $10,000 \text{ events} / 30 \text{ bins} = 333 \text{ events} / \text{bin}$ . Assuming the error on any bin goes as  $\sqrt{N}$ , this gives us just over 5% error / bin. When we were satisfied with the number of events we had collected, we terminated the experiment and saved our results for off-line analysis.

## 4 Results

### 4.1 Calibration

Our raw data is presented in Table 1 and Figure 5. Using Gnuplot we fitted a line to our data to interpolate measurements between the points we recorded. The parameters of our fit are summarized in Table 2.

### 4.2 Counter characterization

The raw data from our bias voltage exercises are presented in Tables 3, 4, 5 and 6. The graphs of these raw data contained many changes in slope; this made finding the common plateau voltage quite difficult. To make our determination we used an analytical approach:

we produced “derivative” plots by graphing the difference between two measurements. Figures 7, 8, 9 and 10 are the plots used to make our determination. We looked for a coincident “dip” in these plots, a bias voltage around which the curves took on a local minimum. This coincident local minimum corresponded to the plateau voltage for a particular PMT.

The raw data from our counter efficiency measurements are presented in Tables 7, 8, 9 and 10. These data are plotted in Figures 11, 12, 13 and 14. We choose the “knee” point of these curves by inspection of the plots; a point where we would achieve the best compromise between signal-to-noise ratio and counter efficiency. This is illustrated in the case of counter A by looking first at Table 3 (noting the noise rate increases with threshold) and then at Figure 11 (noting the efficiency decreases with an increase in threshold). Our choices of bias voltages and discriminator thresholds are summarized in Table 11. Our check of single and double coincidence rates are summarized in Table 12.

### 4.3 Measurement

The MCA software output contained decay counts in 2048 bins. Many bins contained 10 or less events, producing error bars of 30% and greater! To reduce the error in each bin we used ROOT to re-bin the data into 30 bins; these results are displayed in Table 13. In choosing the number of bins with which to re-bin our original data, we used the value  $\chi^2/\nu$  from fits of many different binning scenarios (from 10 to 100 bins) to select our final result; our choice was made by selecting the bin count that produced the smallest result for  $1.0 - (\chi^2/\nu)$ . The re-binned histogram with a curve fit is shown in Figure 15.

It should be noted that my colleague, John Wray, reported two separate results in his determination of  $\tau_\mu$ . While one result was determined from a 30 bin data set, the second result was determined from a much coarser binning scenario (approx. 10 bins). I chose not to report a second result as I did not feel this contributed any greater understanding of the results. Furthermore, using fewer bins will obscure any nuances in the data (i.e. spurious peaks or deviations from exponential behavior) that might illuminate our results.

## 5 Analysis and Interpretation

### 5.1 Theory

Once our experiment was configured (as described in Section 3) we did a quick check of coincidence rates. Empirical data from horizontal detector based experiments yields a  $>1$  GeV muon intensity at sea level of about 1 count /  $\text{cm}^2 \cdot \text{min}$ . With this intensity, our 60 x 25 cm detectors should give a signal rate of 25 Hz (see Equation 3). Our observed double coincidence rates (see Section 4.2 for setup and Table 12 for results) agreed with this result very well; from this we concluded our experiment was in fact properly configured.

$$r_{CR} \approx (60\text{cm} \cdot 25\text{cm}) \cdot 1 \frac{\text{count}}{\text{cm}^2 \cdot \text{min}} \cdot \frac{1\text{min}}{60\text{sec}} = 25\text{Hz} \quad (3)$$

Given the single counter rates we calculated the rate of accidental double coincidences caused by the overlapping of two noise signals:  $r_{acc} = N_1 \cdot N_2 \cdot 2 \cdot \tau$  where  $N_1$  and  $N_2$  are the single rates and  $\tau$  is the pulse width. For our measured single rates, we saw a maximum accidental rate of  $35 \text{ Hz} \cdot 100 \text{ Hz} \cdot 2 \cdot 50 \text{ nS} = 3.5 \text{ mHz}$  (that’s milliHertz!). The rate

of accidental events (two accidental double coincidences within 10 uS) was calculated in a similar fashion, and was determined to be 5.28 mHz. Being that this rate was about four orders of magnitude less than the muon flux through our detectors (compare to Table 12), we concluded the accidental background was not significant enough to cause any worry.

## 5.2 Experiment

The data from our experiment followed the statistical law of radioactivity. To find the mean lifetime from our data, we fit a modified decay equation (see Equation 4) to our histogram. We included a constant term  $B$  to account for our accidental background, since it is equally probable that an accidental event would appear in any bin. Note that  $N_0$  represents the number of counts in bin zero.

$$N = N_0 e^{-\frac{t}{\tau}} + B \quad (4)$$

ROOT was used to perform the fit, see the results in Table 14. ROOT uses a weighted sum-of-squares algorithm to make its fit. A cut was made to improve our fit results since our preliminary fits were grossly inaccurate. In order to achieve a good fit we had to cut the first (leftmost) two bins out of our rebinned histogram before we could achieve acceptable  $\chi^2$  values. This leads us to believe there is some systematic error occurring in the low end of our histogram that is skewing our data. Seeing that our final result is more than  $1 \sigma$  below the currently accepted value for  $\tau_\mu$  reinforces our belief that a systematic error is present and unaccounted for in our theoretical model of the experiment.

It was suggested by a colleague (Prof. Hartmut F.W. Sadrozinski) that timing jitter may be present in our signals going into the TAC. If jitter is in fact present, this error would be most significant in the bins that represent the smallest Time Of Flight (TOF): the low end of our histogram. We could not confirm nor deny the presence of this error due to our lack of knowledge on the subject, nor could we develop a model of this error to include in our fitting equation. Assuming this error is Gaussian in distribution, we should be able to safely ignore its effects. If this error is non-Gaussian, then our results are surely skewed.

ROOT propagated statistical error through its fit, using  $\sqrt{N}$  as the error on each bin. We neglected the errors from our linear interpolations of TAC and MCA measurements due to the low error in the slope parameter; this error was about one part in 1,750, much less than the error in our experimental data (one part in 35 at best, assuming  $\sqrt{N}/N$  error). In re-binning the MCA output, we eliminate most uncertainties in the x-axis (bin number), so the  $\sim 50\%$  error in the intercept parameter is inconsequential. ROOT also produced a chi-square value to describe its fit. Our result of  $\chi^2/\nu = 1.03$  gives us no reason to believe ROOT's fit does not describe our data.

The greatest possible source of systematic error comes from our calibration of the TAC. We felt this calibration exercise was trivial, but did not realize its importance until long after the experiment had been completed. While we took precautions in our logic setup to ensure a uniform "electrical length" existed between start and stop signals, we did not take the same measures in our TAC calibration. Our failure to account for signal delays due to cabling would leave us to believe we are observing a different TOF than that which is presented to the TAC. Since this calibration is required to map the MCA's output to an

actual TOF, any errors in calibration will lead to a skewed final result. Re-calibrating the TAC should reduce our error, but we did not have time to repeat this exercise.

Another source of systematic error comes from re-binning our results. ROOT uses the bin center (or mean bin value) as the x-axis value in performing its fit. With fewer bins, this value is skewed further from the actual values obtained in the experiment. We will get the greatest skew where our curve fit has its greatest slope: at the low end of our histogram. This can be determined by inspection; drawing rectangles to represent each bin, one sees more area between the rectangle and our curve fit where the curve is steep, and less where the curve is flat. A possible method of resolving this error is using the median bin value as the x-axis value used in the fit. Since we could not determine how to make this change to the fitting algorithm in ROOT, we did not explore this option.

## 6 Conclusion

This lab was an excellent introduction to experimental particle physics. The painful amount of data taking and re-taking during counter characterization yielded an intimate knowledge of the workings of these measurement devices, which will prove useful in future experiments involving particle detection. The process of waiting for our data was equally tense and exciting, and our final result was quite satisfactory. The latest issue of Physics Letters (see Reference [1]) lists the muon lifetime at 2.197  $\mu\text{s}$ ; our result is only 4.3% below the agreed lifetime!

## 7 Tables and Figures

Pulse Delay ( $\mu\text{s}$ )	MCA Bin
0.50	104
0.75	155
1.00	207
1.25	258
1.50	309
1.75	361
2.00	412
2.50	513
3.00	615
3.50	721
4.00	822
5.00	1028
6.00	1234
8.00	1645

Table 1: Results of TAC / MCA calibration

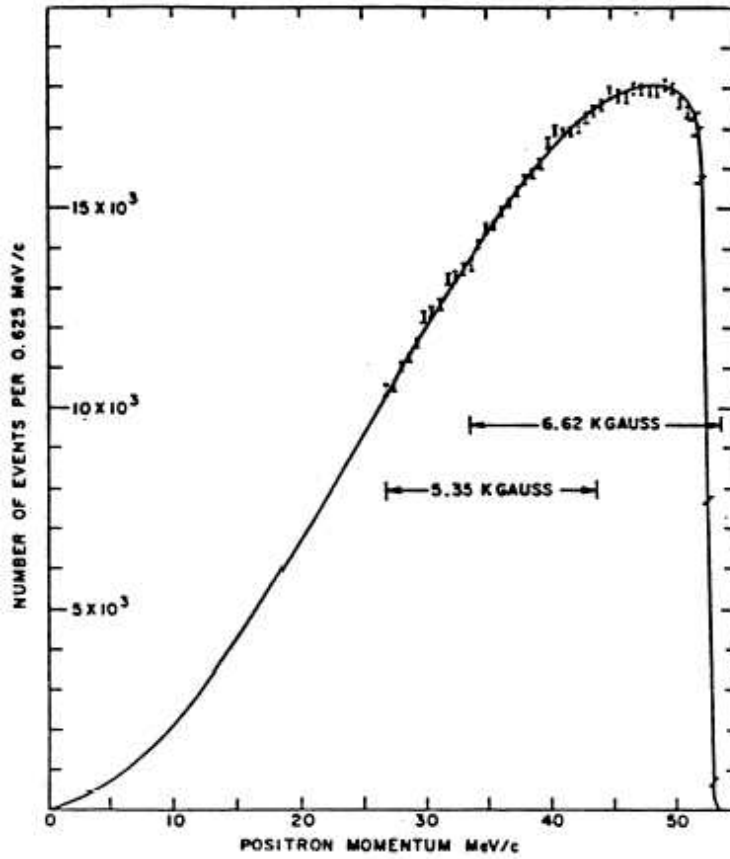


Figure 1: The distribution of electron kinetic energies in muon decay at rest. Data from the experiment of Bardon *et al.* (1965). Experimental points are compared to a modified theoretical curve.

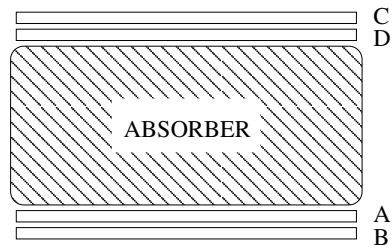


Figure 2: Detail of experimental setup, side view. Counters C and D are above absorber, counters A and B are below. Absorber is described in Section 2.1.

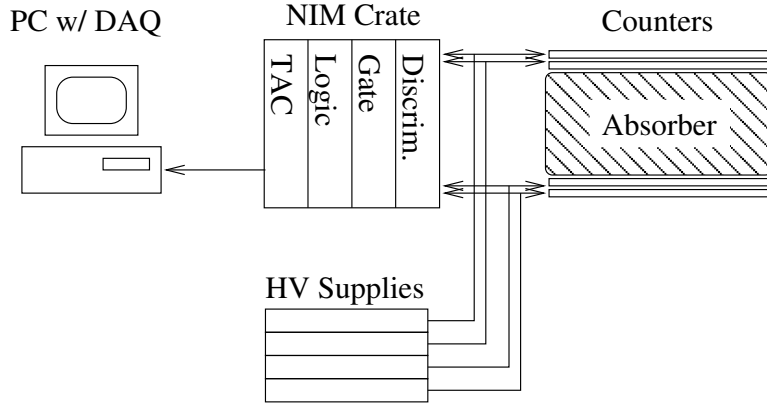


Figure 3: Schematic of experimental setup. Connections within the NIM crate are described in Section 3.3.

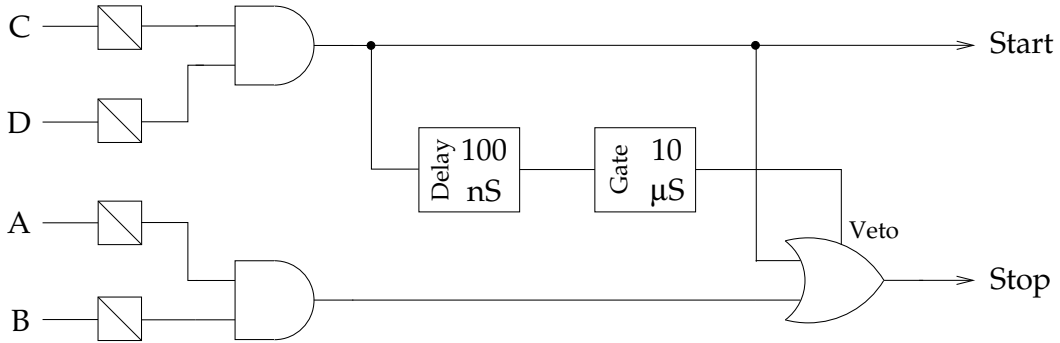


Figure 4: Schematic of electrical configuration. Inputs from PMTs are indicated at left, outputs to TAC appear at right.

Parameter	Value	Error +/-	Error %
Slope	205.456	0.1173	0.0571
Intercept	0.834415	0.422	50.58

Table 2: Details of linear fit

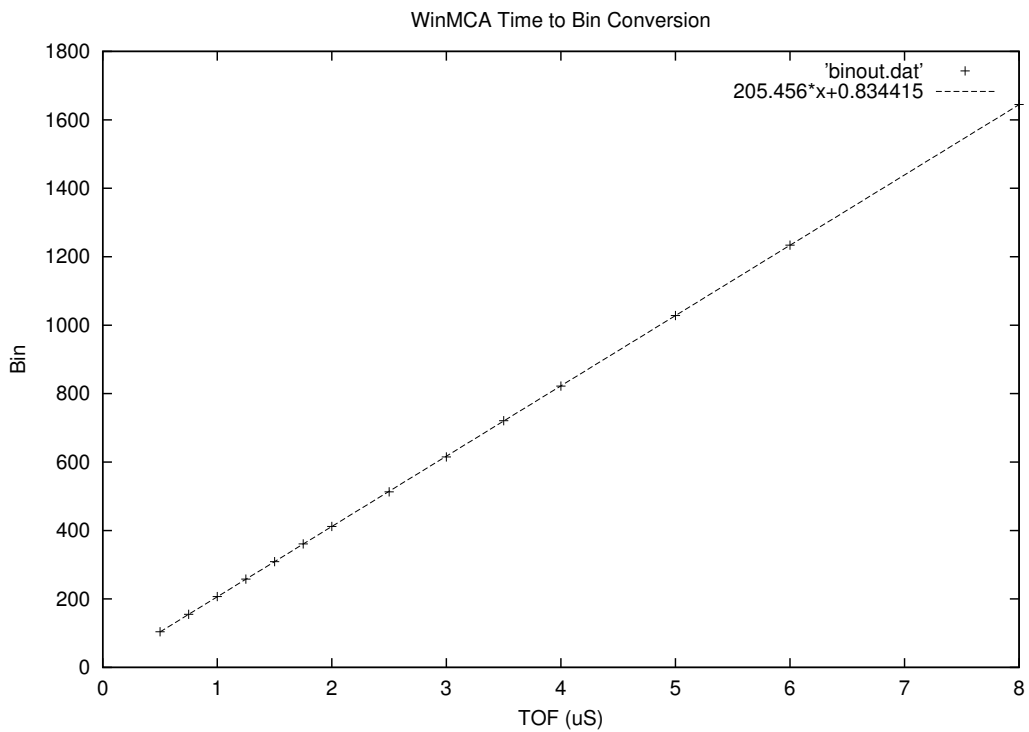


Figure 5: Results of TAC / MCA calibration, plus linear fit (note: TOF is Time Of Flight)

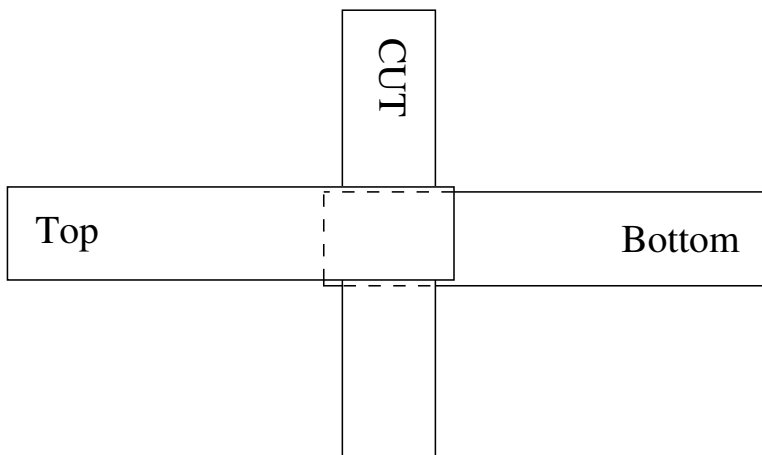


Figure 6: Schematic of counter efficiency calibration

Bias Voltage (V)	-30 mV Counts	-60 mV Counts	-90 mV Counts
1200	32	0	0
1225	48	5	0
1250	92	7	1
1275	160	11	5
1300	264	24	10
1325	471	58	13
1350	659	97	35
1375	1009	189	53
1400	1324	316	106
1425	1772	411	163
1450	2189	672	243
1475	2853	957	400
1500	3699	1247	576
1525	4785	1552	826
1550	6382	1951	1068
1575	7116	2418	1437
1600	8363	3065	1759
1625	9839	3904	2220
1650	12643	5090	2339
1675	13953	6240	3467
1700	16834	7163	4099
1725	20157	8534	5147
1750	22613	10025	6252
1775	28725	12112	7418
1800	30455	14625	8619

Table 3: Results of 100 sec. of measurement with PMT A at three thresholds

Bias Voltage (V)	-30 mV Counts	-60 mV Counts	-90 mV Counts
1200	82	8	3
1225	115	13	2
1250	254	26	13
1275	430	49	7
1300	739	85	22
1325	1160	163	46
1350	1683	283	84
1375	2147	514	175
1400	3056	841	297
1425	4059	1207	387
1450	5920	1669	602
1475	7664	2278	965
1500	11757	3168	1324
1525	14254	4551	1855
1550	22916	6723	2361
1575	34139	10125	3694
1600	54597	14468	5897
1625	91058	19340	8131
1650	167114	26206	10643
1675	208546	34756	15214
1700	274816	50375	20066
1725	351244	77343	26795
1750	440048	120388	36269
1775	509062	169676	51581
1800	588584	245054	83480

Table 4: Results of 100 sec. of measurement with PMT B at three thresholds

Bias Voltage (V)	-30 mV Counts	-60 mV Counts	-90 mV Counts
1200	1	0	0
1225	2	0	0
1250	4	0	0
1275	13	2	0
1300	20	1	0
1325	38	1	0
1350	67	7	2
1375	107	11	2
1400	235	21	7
1425	426	33	10
1450	669	56	10
1475	979	87	20
1500	1327	171	44
1525	1800	279	69
1550	1982	430	122
1575	2423	663	191
1600	3055	937	350
1625	4308	1288	511
1650	7041	1659	831
1675	12919	1753	988
1700	34102	2316	1479
1725	69901	2841	1845
1750	133131	3793	1995
1775	213290	6294	2353
1800	264180	17858	2947

Table 5: Results of 100 sec. of measurement with PMT C at three thresholds

Bias Voltage (V)	-30 mV Counts	-60 mV Counts	-90 mV Counts
1200	0	0	0
1225	0	0	0
1250	0	0	0
1275	0	0	0
1300	2	1	0
1325	1	0	0
1350	1	0	0
1375	3	0	0
1400	6	1	0
1425	13	1	0
1450	25	1	0
1475	53	5	0
1500	80	8	2
1525	125	11	1
1550	232	14	6
1575	373	30	10
1600	565	59	12
1625	782	91	29
1650	1071	132	42
1675	1166	221	53
1700	1617	344	118
1725	1952	543	161
1750	2476	768	210
1775	3265	969	381
1800	3794	1223	524
1825	4650	1441	733
1850	5463	1661	1014
1875	6214	2074	1265
1900	7242	2668	1498

Table 6: Results of 100 sec. of measurement with PMT D at three thresholds

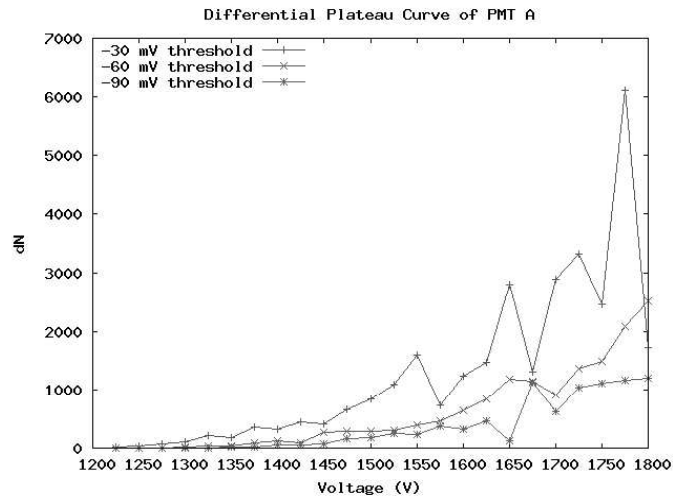


Figure 7: Plot of 100 sec. measurements for PMT A

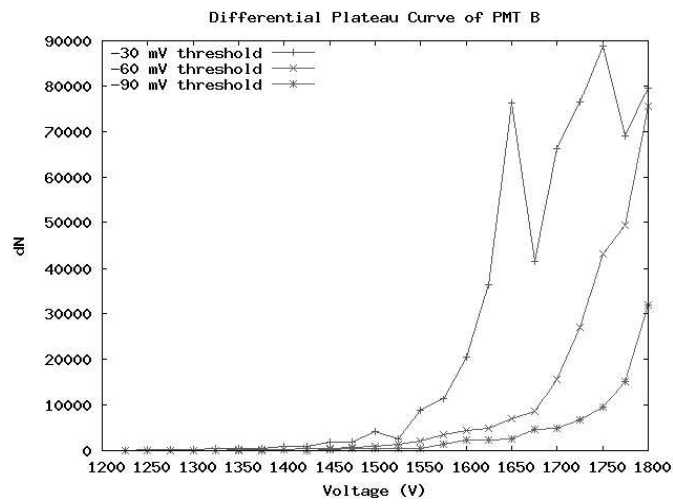


Figure 8: Plot of 100 sec. measurements for PMT B

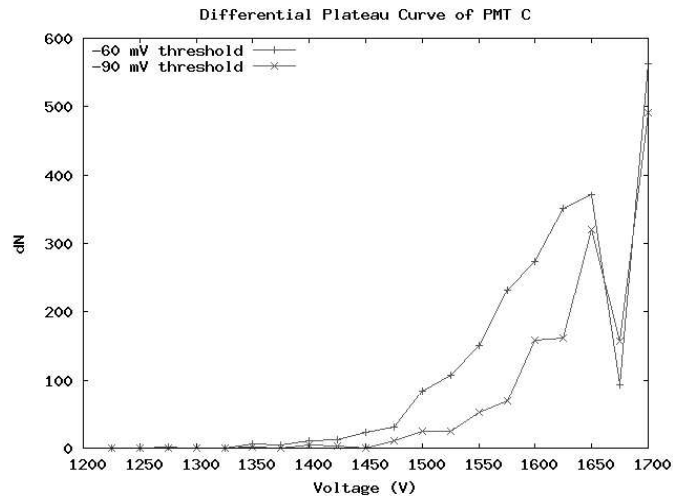


Figure 9: Plot of 100 sec. measurements for PMT C

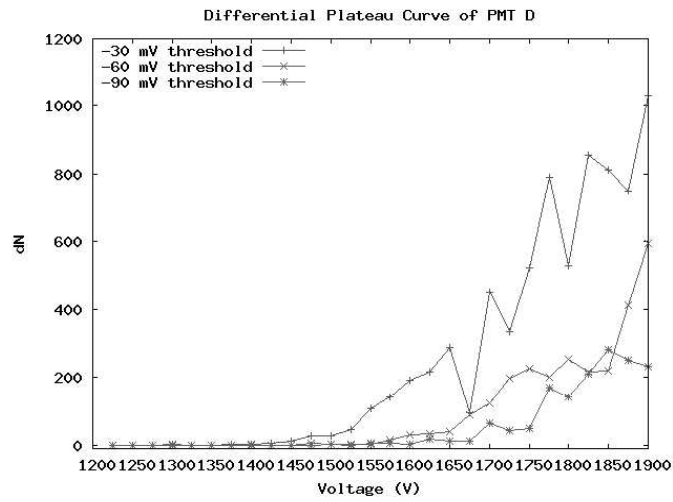


Figure 10: Plot of 100 sec. measurements for PMT D

Threshold (mV)	Triple coinc. count	Double coinc. count	Ratio 3 / 2
50	911	1000	0.911
75	910	1000	0.910
100	897	1002	0.895
125	891	1000	0.891
150	833	1000	0.833
175	756	1001	0.755
200	699	1106	0.632
225	502	1004	0.500
250	370	1000	0.370
275	259	1001	0.259
300	247	1000	0.247

Table 7: Efficiency measurements for counter A

Threshold (mV)	Triple coinc. count	Double coinc. count	Ratio 3 / 2
50	946	1002	0.944
75	931	1003	0.928
100	933	1001	0.932
125	930	1002	0.928
150	917	1001	0.916
175	870	1004	0.867
200	820	995	0.824
225	757	1004	0.754
250	687	1006	0.683
275	566	1001	0.565
300	491	1006	0.488

Table 8: Efficiency measurements for counter B

Threshold (mV)	Triple coinc. count	Double coinc. count	Ratio 3 / 2
50	966	1002	0.964
75	947	1003	0.944
100	860	1001	0.859
125	630	1002	0.629
150	441	1002	0.440
175	283	1003	0.282
200	199	1004	0.198

Table 9: Efficiency measurements for counter C

Threshold (mV)	Triple coinc. count	Double coinc. count	Ratio 3 / 2
50	913	1002	0.911
75	636	1001	0.635
100	332	1004	0.331
125	188	1005	0.187
150	104	1011	0.103
175	64	1003	0.064
200	53	1001	0.053

Table 10: Efficiency measurements for counter D

Counter	Bias Voltage (V)	Threshold (mV)
A	1700	-110
B	1675	-135
C	1675	-60
D	1725	-30

Table 11: Operating parameters for counters

Coinc.	Counter(s)	Rate (Hz)
Single	A	35
Single	B	100
Single	C	50
Single	D	35
Double	A+B	22
Double	C+D	24

Table 12: Coincidence rates from counters in experimental configuration

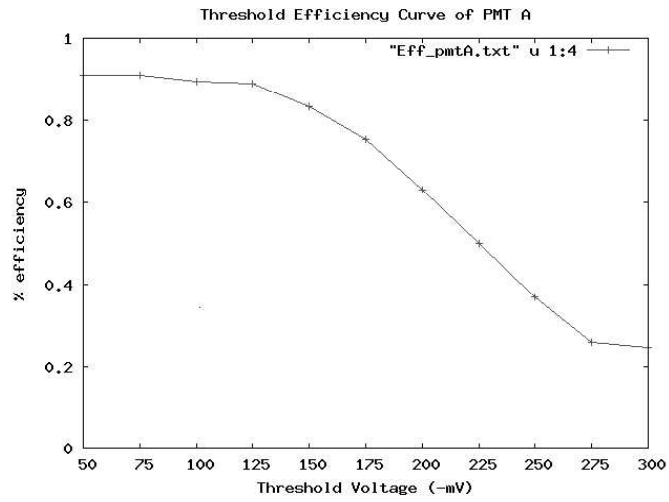


Figure 11: Plot of efficiencies of PMT A

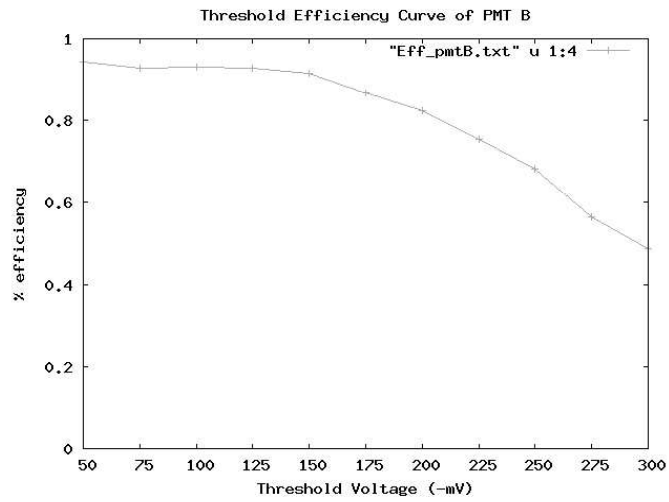


Figure 12: Plot of efficiencies of PMT B

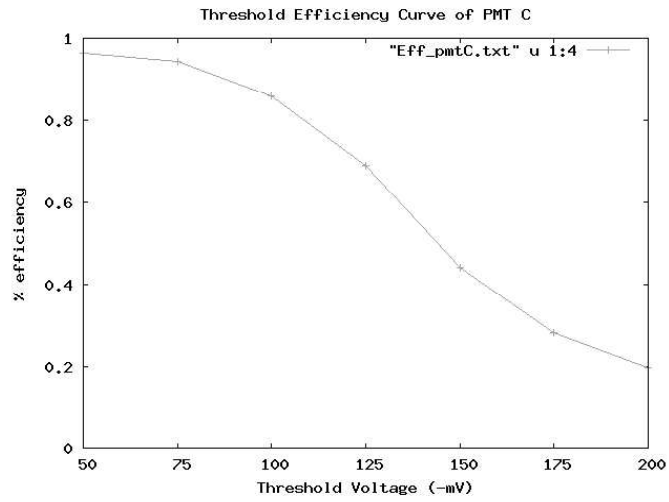


Figure 13: Plot of efficiencies of PMT C

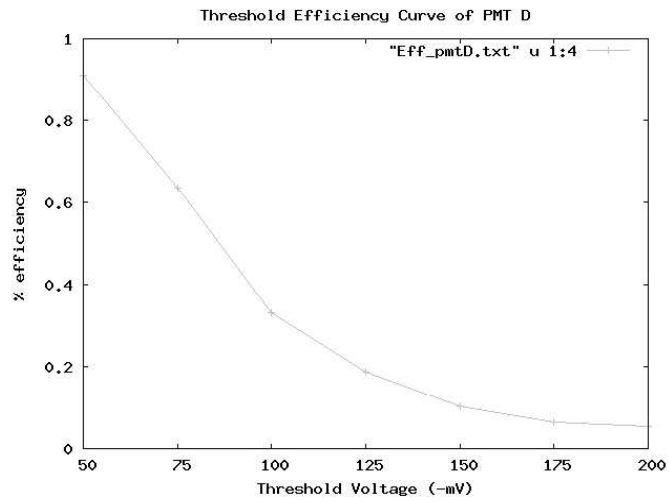


Figure 14: Plot of efficiencies of PMT D

Bin	Time ( $\mu$ S)	Counts
1	0.76	1171
2	1.07	1022
3	1.38	874
4	1.70	773
5	2.01	654
6	2.32	551
7	2.64	490
8	2.95	431
9	3.26	358
10	3.58	333
11	3.89	291
12	4.20	217
13	4.52	225
14	4.83	191
15	5.14	192
16	5.46	135
17	5.77	120
18	6.08	133
19	6.40	117
20	6.71	104
21	7.02	98
22	7.34	90
23	7.65	66
24	7.96	77
25	8.28	57
26	8.59	62
27	8.90	45
28	9.22	51
29	9.53	51
30	9.84	32

Table 13: Re-binned results of experiment

Parameter	Value	Error +/-	Error %
$N_0$	7.40	0.024	0.3
$\tau$	2.10	0.05	2.5
$B$	28.5	3.9	13.6
$\chi^2$	27.9		
$\nu$	27		
$\chi^2/\nu$	1.03		

Table 14: Details of curve fit

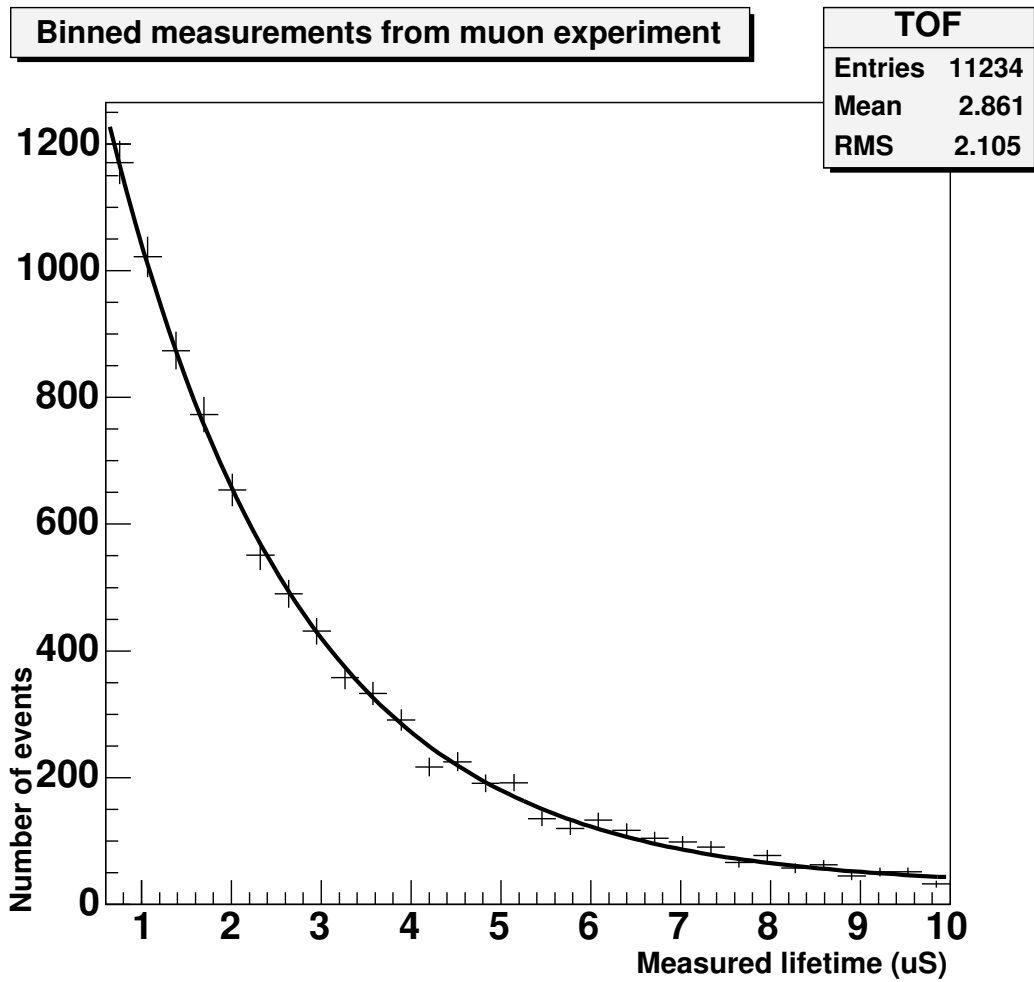


Figure 15: Results of experiment, with curve fit

## Acknowledgments

My highest praises go to Dave Dorfan for teaching physics like no other professor on the planet. His instruction through this experiment has been insightful, compelling and entertaining, to say the least. Many kudos go to Fred Kuttner for making our lab experience pleasant and free of hassle. Thanks to my partner John Wray for contributing his analytical and experimental skills to this project.

## References

- [1] S. Eidelman *et al*, Phys. Lett. B **592**, 1 (2004)
- [2] P. Tipler and R. Llewellyn, *Modern Physics*, 3rd ed. New York: W. H. Freeman and Co., 1999.
- [3] D. Dorfan, “Notes for the Muon Lifetime Experiment” handout. University of California at Santa Cruz: 2004.
- [4] R. Schumacher and R. Edelman, “Cosmic Ray Muons” handout. Carnegie Mellon University: 2002.